Experimental investigation of cohesive soil erosion and suspension caused by a Coandă-effect-based polymetallic-nodule collector

Alhaddad, S.M.S.; Suleman, M.; Kirichek, Alex ; Chassagne, C.

DOI
10.1016/j.rineng.2024.102231

Publication date
2024

Document Version
Final published version

Published in
Results in Engineering

Results in Engineering 22 (2024) 102231

Contents lists available at ScienceDirect

Results in Engineering

journal homepage: www.sciencedirect.com/journal/results-in-engineering

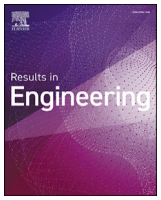

Research paper

Experimental investigation of cohesive soil erosion and suspension caused by a Coandă-effect-based polymetallic-nodule collector

Said Alhaddad [a,*], Mohammed Suleman [b], Alex Kirichek [c], Claire Chassagne [b]

[a] Section of Offshore and Dredging Engineering, Faculty of Mechanical Engineering, Delft University of Technology, Delft, the Netherlands
[b] Section of Environmental Fluid Mechanics, Faculty of Civil Engineering and Geosciences, Delft University of Technology, Delft, the Netherlands
[c] Section of Rivers and Ports, Faculty of Civil Engineering and Geosciences, Delft University of Technology, Delft, the Netherlands

ARTICLE INFO

Keywords:
Sediment erosion
Deep sea mining
Polymetallic nodules
Coandă effect
Impinging jet
Turbidity current

ABSTRACT

Coandă-effect-based collection stands out as the foremost technology in polymetallic-nodule mining due to the absence of direct contact between the collector and the ocean floor. Yet, this collection method disturbs the ocean floor, and minimizing such disturbance is crucial from an environmental viewpoint. To this end, a solid understanding of the interplay between the collector and the sediment bed is required. Therefore, we carried out a series of small-scale experiments, where a collector drives over a subaqueous clayey bed. These experiments provide the very first quantitative data on cohesive sediment erosion caused by a moving Coandă-effect-based collector, as well as on turbidity currents generated behind the collector head. This paper discusses the observations and findings derived from these experiments. Our findings reveal a logarithmic relationship between erosion depth and the flow impinging force applied on the clayey bed. An increased flow rate in the collection duct results in a slower turbidity current generated behind the collector head. This study enhances the ability to forecast sediment erosion caused by Coandă-effect-based collectors, offering the possibility to optimize the collector operational conditions and minimize the magnitude of the resulting sediment plumes.

1. Introduction

The global demand for specific metals (e.g., copper and cobalt) has been steadily increasing due to the urgent necessity for transitioning towards a decarbonized future. These metals play a pivotal role in driving the electrification of the transportation sector, particularly in the production of battery-powered vehicles. With terrestrial mineral deposits facing depletion, there has been a growing focus among industrialists and scientists on the deep-sea floor [18]. Vast reserves of strategic metals and rare-earth elements are embedded in the ocean floor, particularly within potato-sized concretions known as polymetallic nodules [16]. These nodules have high concentrations of valuable metals (e.g., cobalt, copper, manganese, and nickel) and are typically found at water depths ranging from 4 to 6 kilometers across all oceans. Notably, nodules are widely scattered across the ocean floor within the Clarion Clipperton Zone (CCZ) [10].

Coandă-effect-based collection stands out as the leading technology in polymetallic-nodule mining due to its avoidance of direct contact between the collector and the ocean floor [20,5]. However, such collectors disturb the seabed; sediment is inevitably picked up and collected together with the nodules during the mining process. The collected sediment is discarded at the rear of the collector, forming a sediment plume traveling across the ocean floor [8,1]. This plume could possibly drift for long distances, considerably disrupting aquatic ecosystems in its way [14]. Aiming for the least environmental impact, the sediment pick-up, and, by extension, the sediment concentration of the sediment-water mixture discarded at the collector rear must be minimized. To this end, a solid understanding of the interplay between the collector and the sediment bed is required.

Alhaddad and Helmons [3] conducted a set of small-scale experiments to explore the pick-up of sand by a moving Coandă-effect-based collector. They found out that the erosion depth is logarithmically proportional to the impinging force exerted by water flow on the sand bed. Given that deep-sea sediment, on/in which polymetallic nodules are available, is mainly composed of clay [9], it is worth exploring whether such a correlation also holds. Alhaddad and Helmons [3] also revealed that water spilling behind the collector head generates a turbidity current (particle-laden gravity-driven underflow). However, in

* Corresponding author.
E-mail addresses: S.M.S.Alhaddad@tudelft.nl (S. Alhaddad), mo-suleman@outlook.com (M. Suleman), o.kirichek@tudelft.nl (A. Kirichek), c.chassagne@tudelft.nl (C. Chassagne).

https://doi.org/10.1016/j.rineng.2024.102231
Received 4 April 2024; Received in revised form 3 May 2024; Accepted 3 May 2024
Available online 9 May 2024

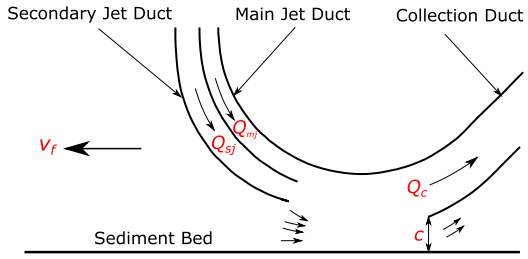

Fig. 1. Schematic representation of the collector head [3]; v_f is the forward velocity of the collector, c is bottom clearance, Q_{mj}, Q_{sj} and Q_c are the flow rates through the main-jet duct, the secondary-jet duct and the collection duct, respectively. The small arrows above the bed depict the direction of water entrainment and water spillage behind the collector head.

their experiments they have not sought to measure or investigate the generated turbidity currents. Noteworthy to mention is that turbidity currents can also originate from other anthropogenic activities besides polymetallic-nodule mining, such as dredging operations [6,4] and tailing discharges [11].

The objective of this study is to explore and quantify cohesive sediment erosion generated by a Coandă-effect-based polymetallic-nodule collector as well as turbidity currents generated behind the collector head. To this end, we performed small-scale experiments in a water flume where a collector drives over an underwater clayey bed. We investigate how key operational parameters, such as main jet velocity, secondary jet velocity, collector's forward velocity (the speed at which the collector moves over the seabed), and bottom clearance impact the level of disturbance to the clayey bed. Furthermore, our measurements are used to investigate the underlying physics that control the depth of the disturbed bed caused by the collector. We also explore how the dynamics of turbidity currents generated behind the collector head change under the various operational conditions tested in this study. Finally, the article discusses the implications of our findings for collector operation, highlighting strategies to reduce the scale of sediment plumes. It is worth noting that the measurements acquired within this study may also be used for the validation of numerical models employed for the enhancement of the collector design.

2. Coandă-effect-based collector

The collector considered in our study utilizes the Coandă effect, a fluid-mechanical phenomenon, where a jet flow adheres to an adjacent surface even if it curves [15]. The collector consists of four curved surfaces forming three ducts: the main-jet duct, the secondary-jet duct, and the collection duct (see Fig. 1). As a result of the Coandă effect, high-velocity water jets flow along the upper curved plate and entrain ambient water toward the collection duct. This creates a suction under the collector, dislodging nodules from the bed, which are subsequently dragged by the flow towards the collection duct [5]. The idea behind using a secondary-jet duct in the full-scale, real-life collector is to allow sediment-water circulation over the duct within the collector head, which reduces the discharge rate of sediment-water mixture at the collector rear.

Due to ambient water entrainment, the collector ejects water behind the collector head (termed as the 'spilling water'), which flows in the opposite direction of the collector movement, with sufficient velocity to carry sediment particles in suspension. This, in turn, results in the formation of an additional turbidity current, which will eventually interact with the turbidity current resulting from the mixture discharge behind the collector itself.

3. Laboratory experiments

This section describes the experimental setup, instrumentation, test procedure and characterization of clay, respectively.

3.1. Experimental setup

The experimental setup has been designed to investigate the influence of the collector head on a clayey bed. Experimental components include the collector head, mobile carriage, PVC hoses, water pumps, and a water flume. The collector head, mounted on a mobile carriage, undergoes controlled motion along a 5-meter rail atop the water flume with a controllable velocity. A wooden tray within the flume is used for the systematic application of clay to the bed. A separate tank is used to collect the sediment-water mixture flowing through the collection duct.

The collector head used in this study is detailed in Alhaddad et al. [5]. It is equipped with two jet ducts (main and secondary) and one collection duct, each connected to individual water pumps (Fig. 2). Variable-frequency drives (VFDs) are employed to regulate flow rates in all three ducts, providing a methodical means to fine-tune experimental conditions.

3.2. Instrumentation

The experimental configuration incorporated two electromagnetic flow meters to monitor the flow rate within the jet hoses, along with an acoustic flow meter dedicated to tracking the flow rate in the collection hose. For the assessment of bed disturbance depth, or 'erosion depth,' three optical sensors (optoNCDT 1302) were affixed to the mobile carriage. These sensors measure the distance from the sensor to the clayey bed as the carriage moves along the water flume. To facilitate underwater use, the optical sensors were securely housed in a bespoke watertight housing. The determination of sensor position and subsequent measurements along the flume was achieved through the utilization of a wheel encoder. Additionally, an Ultrasonic Velocity Profile (UVP) was employed for the purpose of measuring the vertical velocity profile of the turbidity current caused by the spillage underneath the collector head.

3.3. Test procedure and data acquisition

The experiments were conducted by replicating identical steps. This approach ensures a systematic comparison of experimental results, providing reliability and meaningful observations. The sequence of steps for each test is as follows:

- Empty the testing compartment from water using two submersible pumps.
- Fill the prepared clay in the wooden tray to a depth of 50 mm.
- Level the clayey bed with a wooden plate.
- Add water until reaching a water level of 360 mm, leaving a 70 mm clearance between the water surface and the top of the flume.
- Measure the initial bathymetry using optical sensors by driving the mobile carriage forward and then backward to the starting point. This process is repeated twice, making six scans using three lasers each time.
- Turn on the water pumps. Variable-frequency drives (VFDs) are used to obtain the target flow rate in each duct.
- Drive the mobile carriage forward at the required velocity and stop at the end of the rails using sensors mounted at each endpoint.
- Slowly empty the flume using the submersible pumps.
- Clean the testing compartments from clay chunks using a wet vacuum cleaner, leaving the eroded clayey bed untouched.
- Fill the flume slowly and carefully with clean water to avoid disturbing the clayey bed, enabling the optical sensors to measure the bed effectively.
- Drive the carriage along the flume again to measure the final bathymetry. This process is repeated five times, making a total of fifteen scans.

The erosion analysis involves measuring the change in bathymetry, and a cross-sectional profile is determined using the average values of

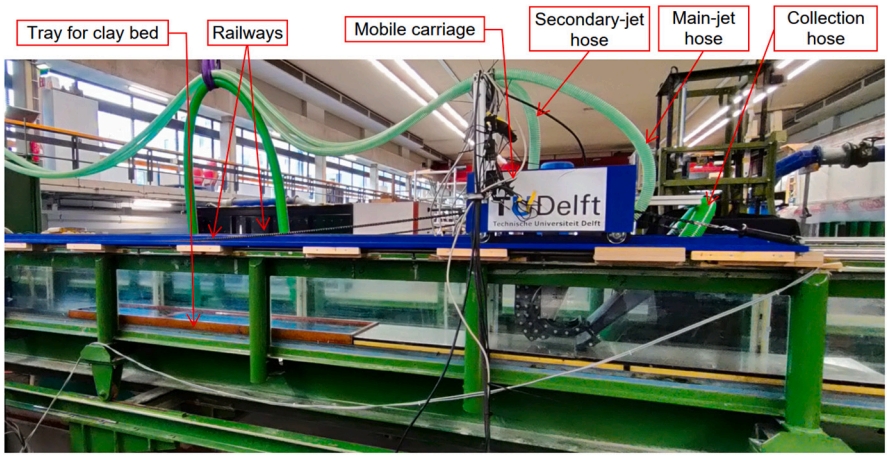

Fig. 2. Front view of the experimental setup showing most of the equipment used.

Table 1
A summary of the experiments conducted within this study. v_{mj}, v_{sj}, and v_c represent the flow velocities through the main-jet duct, the secondary-jet duct, and the collection duct, respectively, while e_m denotes the maximum erosion depth.

Test #	Q_{mj} [L/s]	Q_{sj} [L/s]	Q_c [L/s]	v_{mj} [m/s]	v_{sj} [m/s]	v_c [m/s]	c **[mm]**	v_f [cm/s]	e_m [mm]
1	4.4	6.1	10.5	4.4	0.98	1.4	3	50.0	8.9
2	4.4	6.1	10.5	4.4	0.98	1.4	3	37.5	10.0
3	4.4	6.1	10.5	4.4	0.98	1.4	3	25.0	11.8
4	4.4	6.1	10.5	4.4	0.98	1.4	3	12.5	17.6
4r	4.4	6.1	10.5	4.4	0.98	1.4	3	12.5	16.9
5	4.4	6.1	10.5	4.4	0.98	1.4	0	12.5	24.3
6	4.4	6.1	10.5	4.4	0.98	1.4	5	12.5	16.0
7	4.4	6.1	10.5	4.4	0.98	1.4	8	12.5	13.9
8	4.4	0.0	4.4	4.4	0.00	0.6	3	12.5	10.0
9	4.4	3.0	7.4	4.4	0.48	1.0	3	12.5	11.6
10	4.4	4.7	9.1	3.0	0.75	1.2	3	12.5	16.1
11	3.0	6.1	9.1	3.0	0.98	1.2	3	12.5	11.7
12	2.0	6.1	8.1	2.0	0.98	1.1	3	12.5	10.2
13	0.0	6.1	6.1	0.0	0.98	0.8	3	12.5	4.6
14	4.4	no duct	4.4	4.4	no duct	0.6	3	12.5	18.5

the fifteen scans. Table 1 summarises the initial conditions of the experiments conducted within this study. Four different values for each operational parameter are tested, providing ample variations to adequately study the influence of these parameters.

3.4. Characterization of clay

While the terrestrial clay and soft sediment on the seafloor differ significantly in composition, and formation conditions, they exhibit a degree of similarity, as indicated by the findings from the in-situ test conducted in the CCZ [12]. The synthesized clay should replicate the characteristics of deep-sea clay, with particular emphasis on aligning its shear strength properties. It is crucial for the clay to be easily mixable, ensuring a homogeneous and consistent mixture to facilitate reliable experimentation. Moreover, a preference for ease of cleaning is emphasized to mitigate excessive stickiness, which could disrupt the experimental setup. Adhering to these criteria, the prepared clay serves as an apt medium for studying clay erosion, contributing to a more precise representation of real-case scenarios. Drawing inspiration from the work of Shakeel et al. [17], the selected blend comprised 8% bentonite and 92% kaolinite, yielding a total solid content of 45%. This specific composition was chosen for its desirable rheological properties and behaviour aligned with the objectives of the experiments. As indicated in Shakeel et al. [17], this mixture yields a shear strength of 0.1 kPa. Validation of this value was conducted through a rheological analysis (see Fig. 3). Other characteristics of the prepared clay can be found in Table 2.

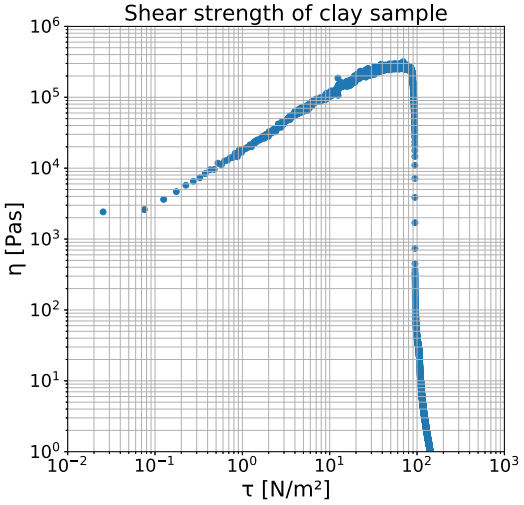

Fig. 3. Shear strength, τ, as a function of the clay viscosity, η, for the used clay.

Table 2
Characteristics of the clay used in the experiments.

σ (kPa)	ρ (kg/m^3)	Solid content (-)	Particle Size (d_x) (μm)			
			d_{10}	d_{50}	d_{60}	d_{90}
0.1	1352	0.43	2.1	5.9	7	14.7

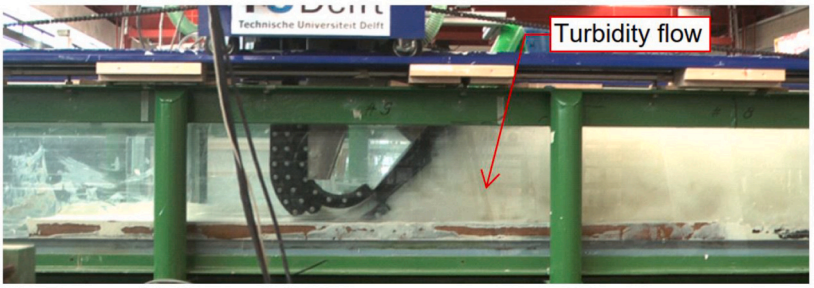

Fig. 4. Experimental run showing the turbidity current behind the collector head.

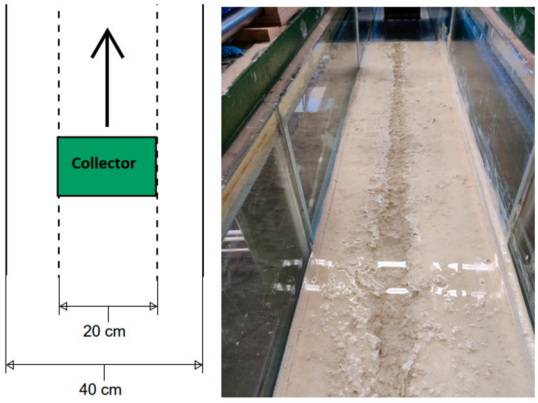

Fig. 5. Top view of the water flume depicting the position of the collector (left). Trench created as a result of clay erosion of Experiment 3 (right).

4. Experimental results

The following subsections will encompass the presentation and analysis of the experimental data in the context of our scientific inquiry.

4.1. General description of sediment erosion

As the collector drives over the clayey bed, it erodes a layer of clay, of which a large portion is captured and directed toward the collection duct. Concurrently, the remaining eroded clay becomes suspended in the water column behind the collector head, creating a turbidity flow (Fig. 4). Notably, not all eroded clay reaches the collection duct. The spilling water, moving counter to the collector's direction, brings clay particles in suspension, which will ultimately settle out on the clayey bed. This results in a deposition layer forming within 1-4 hours after each experimental run, necessitating the flume to be emptied for measurements due to the long settling time.

Clayey bed erosion exhibits variations in both length and width directions (see Fig. 5 right). To visually present this, 15 line scans were taken, and their average values were used to construct a cross-sectional profile of the clayey bed (Fig. 6). This profile aids in determining the maximum erosion depth and eroded clay area, providing valuable insights into the erosion mechanisms. The dashed horizontal line at y = 0 represents the averaged clayey bed position prior to experiments based on six line scans. These scanning steps were applied consistently across all experiments to generate cross-sectional profiles (see Appendix A).

To ensure the reliability and validity of the experimental outcomes, it is critical to confirm their reproducibility under consistent operational parameters. To this end, we have repeated Experiment 4, referred to as Experiment 4r. The maximum erosion depths observed in Experiment 4 and its repetition, Experiment 4r, were 17.6 mm and 16.9 mm respectively. The presence of similar cross-sectional profiles in both experiments serves as robust validation for the obtained results, enhancing the overall trustworthiness of the findings (see Fig. 7). The consistent appearance of the clayey bed's cross-section indicates that the experimental conditions were controlled and reproducible, resulting in uniform erosion patterns.

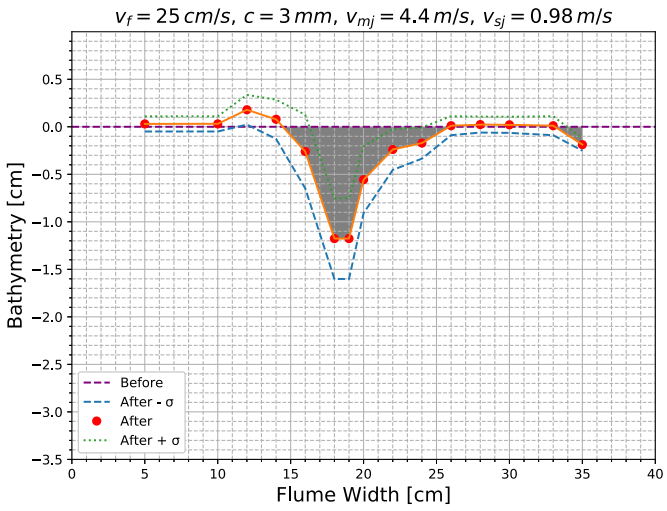

Fig. 6. Cross-sectional profile of Experiment 3 obtained with optical sensors; σ is the standard deviation.

4.2. Flow impinging force

Cohesive sediment erosion is a complex process that involves the detachment and transport of fine-grained particles that have a high degree of inter-particle bonding, such as clay and silt. The cohesive forces between the particles in the sediment can make it difficult for the water flow to detach and transport them, leading to different erosion mechanisms depending on the hydraulic conditions and sediment properties [19].

Alhaddad and Helmons [3] revealed that the erosion depth resulting from the collector is logarithmically proportional to the flow impingement force on a sand bed. Here, we investigate whether such a correlation also holds for cohesive sediment. Fig. 8 depicts a photo taken by a high-speed camera when the collector was operated in a stationary mode ($v_f = 0$). It can be seen that the flow under the collector head impinges on the bed.

The component forces and resultant force read [3]:

$$F_x = \dot{m}(v_j \cos\theta_1 - v_c \cos\theta_2) \quad (1)$$

$$F_y = \dot{m}(-v_j \sin\theta_1 - v_c \sin\theta_2) \quad (2)$$

$$F = \sqrt{F_x^2 + F_y^2} \quad (3)$$

where v_j is the velocity of the water jet when the two jet ducts are combined, θ_1 (40°) is the angle between v_j and X-axis, v_c is the flow velocity in the collection duct, θ_2 (45°) is the angle between v_c and

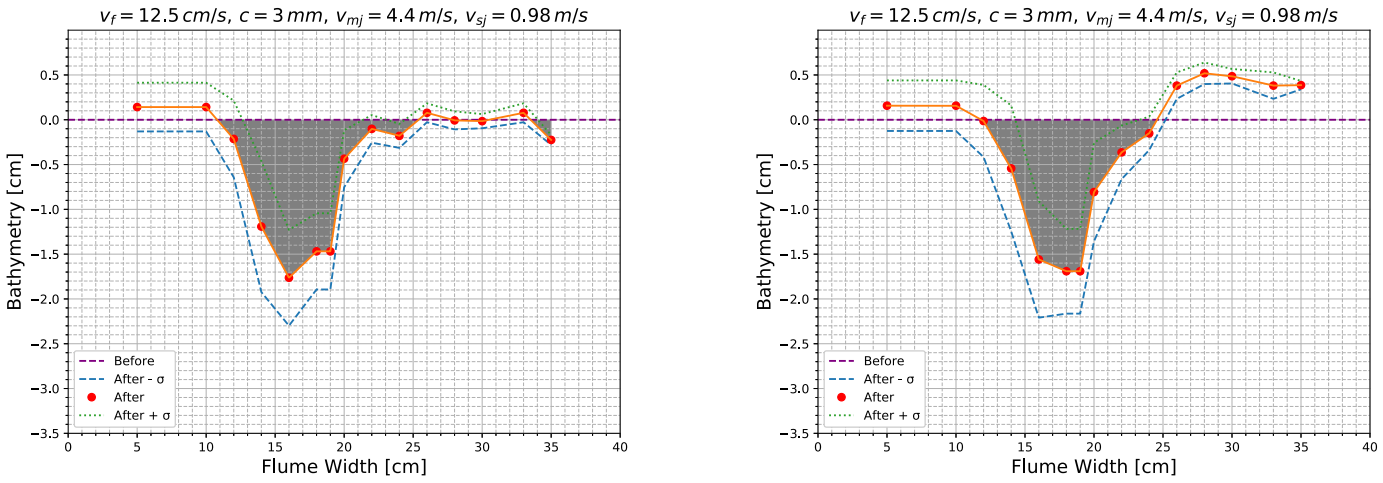

Fig. 7. Cross-sectional profile of Experiment 4 (left) and Experiment 4r (right); σ is the standard deviation.

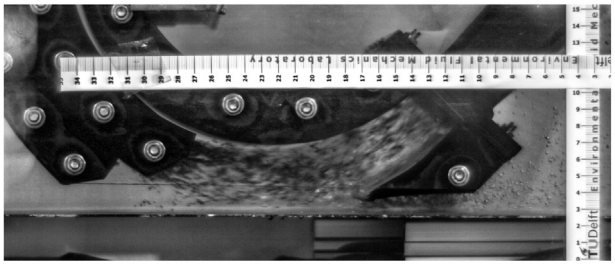

Fig. 8. Image obtained by a high-speed camera illustrating that the flow under the collector head strikes the bed.

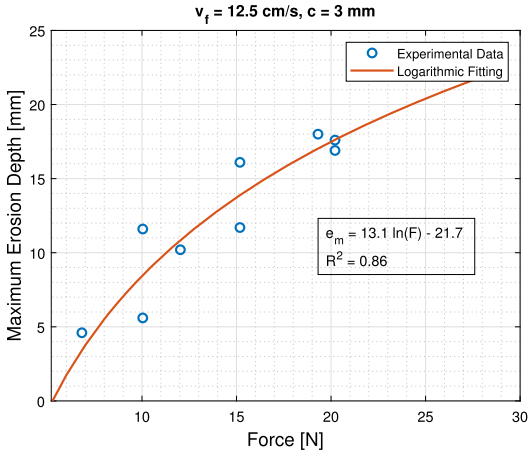

Fig. 9. Logarithmic correlation between the flow impinging force and the maximum erosion depth.

X-axis, and $\dot{m}$ is the mass per unit time entering/leaving the control volume and can be calculated as:

$$\dot{m} = \rho Q_j = \rho Q_c \tag{4}$$

In our analysis, we consider all experimental runs in which v_f = 12.5 cm/s and c = 3 mm as these represent the vast majority of the tests performed. Interestingly, similar to the finding of Alhaddad and Helmons [3], Fig. 9 depicts a logarithmic correlation between the impinging force F [N] and the maximum erosion depth, e_m [mm]:

$$e_m = 13.1 \ln(F) - 21.7 \tag{5}$$

4.3. Main and secondary jets

The investigation of the impact of the main jet velocity, v_{mj}, on clay erosion is conducted through a series of four tests in which the other parameters are held constant. The main jet velocity is systematically varied, with the bottom clearance fixed at 3 mm and the forward velocity maintained at 12.5 cm/s. The flow velocity in the secondary-jet duct is kept constant at 0.98 m/s. It can clearly be seen that a lower v_{mj} results in a smaller erosion depth (see Fig. 10 left). A decrease in v_{mj} leads to a reduction in the impingement force, resulting in shallower but wider erosion patterns. Furthermore, the higher standard deviation of the erosion data indicates non-uniform chunks of the eroded clay, as opposed to a homogeneous pattern.

The exploration of the effect of secondary jet velocity on clay erosion also involves four tests, maintaining constant parameters. The secondary jet velocity is systematically varied, with the bottom clearance fixed at 3 mm and the forward velocity held constant at 12.5 cm/s. Additionally, the flow velocity in the main-jet duct is maintained at 4.1 m/s. An intriguing observation arises when there is little to no flow rate in the secondary jet, resulting in more concentrated and deeper erosion in the middle (Fig. 10 right). This phenomenon suggests that the absence or reduction of the secondary jet velocity alters the distribution and intensity of erosion in the clayey bed. The concentration of erosion in the middle indicates a localized effect likely influenced by the impingement of the main jet. The decrease in erosion depth with a reduction in the secondary jet velocity can be attributed to the decreased impingement force on the clayey bed.

4.4. Presence of secondary-jet duct

To investigate the influence of the presence of the secondary-jet duct on clay erosion, Test 14 was conducted. This test is identical to Test 8 (secondary jet velocity = 0), but with the secondary-jet duct removed, as documented in Table 1. The purpose of Test 14 is to compare the erosion patterns and dynamics in the absence of the secondary-jet duct with the conditions when the duct is present.

Fig. 11 displays the cross-sectional profiles of Test 8 and Test 14, comparing the cases with and without the secondary-jet duct. Notably, Test 14 exhibits much more erosion, indicating that the presence of the secondary-jet duct leads to a decreased erosion depth. To investigate the reason behind this observation, we studied the influence of the presence of the secondary-jet duct on the flow rate through the collection duct in tests where no hose or pump was connected to the collection duct. We found out that the flow rate in the collection duct, Q_c, is higher when the secondary-jet duct is still fastened in place. A higher Q_c indicates an increase in water entrainment.

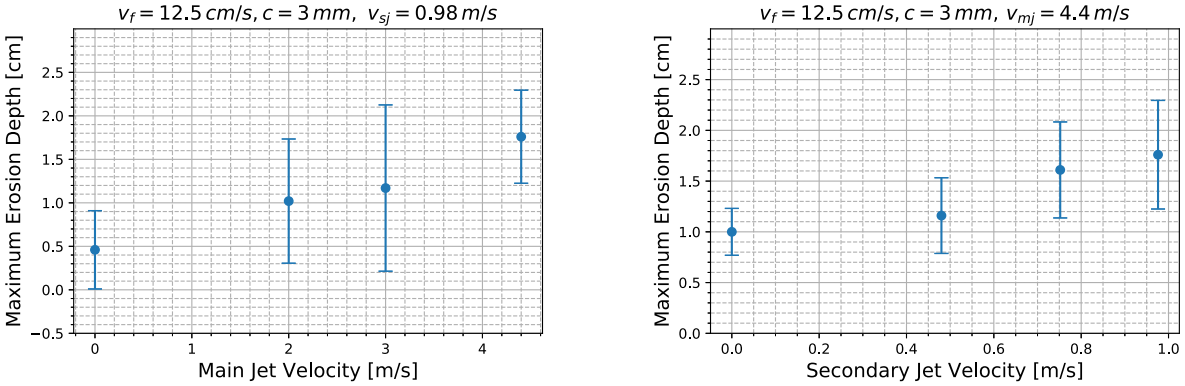

Fig. 10. Effect of the flow velocity in the main jet (**left**) and the flow velocity in the secondary jet (**right**) on the erosion depth.

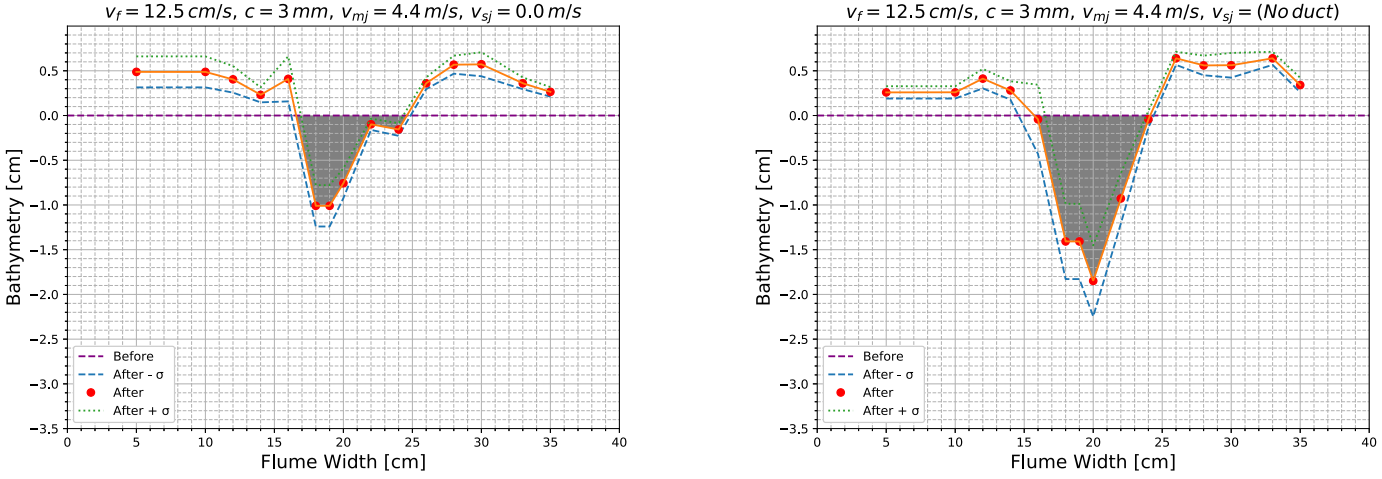

Fig. 11. Cross-sectional profile of Experiment 8 (left) and Experiment 14 (right), where σ is the standard deviation.

The observed increase in water entrainment and decrease in erosion depth when the secondary-jet duct is present can be attributed to the attachment of the flow under the collector head. When the secondary-jet duct is present and switched off ($v_{sj} = 0$), the flow under the collector head adheres more to the curved underside, leading to more water entrainment and no strike on the sediment bed. The latter was also observed by Alhaddad and Helmons [3].

4.5. Collector's forward velocity

In this section, we explore the impact of the collector's forward velocity through a series of four tests. The forward velocity is systematically varied while keeping all other parameters constant. Specifically, the flow velocities in the main-jet duct and secondary-jet duct are maintained at 4.4 m/s and 0.98 m/s, respectively, with a fixed clearance of 3 mm. Notably, our experimental findings clearly demonstrate that a lower v_f results in a greater erosion depth (Fig. 12). This correlation is expected, as a lower v_f implies a longer exposure of the clayey bed to the water jets and thus more erosion.

4.6. Bottom clearance

The investigation of the impact of bottom clearance on clay erosion involves four tests. While keeping all other parameters constant, the bottom clearance is systematically varied, with the forward velocity held constant at 12.5 cm/s. The flow velocities in the main-jet duct and secondary-jet duct are maintained at 4.4 m/s and 0.98 m/s, respectively.

It is noteworthy that Experiment 5 exhibited the highest erosion depth among the tests. Specifically, in this experiment, the bottom clearance was set to 0 mm, resulting in the most significant erosion observed in the clayey bed (Fig. 13). The experimental results unequivocally demonstrate that a smaller bottom clearance corresponds to a larger erosion depth. This correlation aligns with expectations, as a reduced bottom clearance exposes a larger clay layer to the water jets, resulting in more erosion.

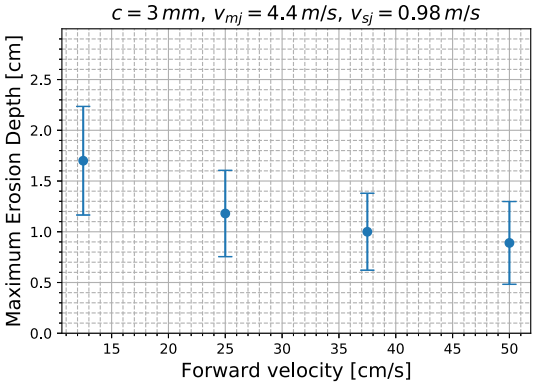

Fig. 12. Effect of collector's forward velocity on the erosion depth.

5. Sediment erosion caused by full-scale collector

Utilizing the measured erosion depths from the conducted experiments, and considering that the collector head is scaled down by a factor of four in 2D dimensions, Froude scaling can be applied to provide first-order predictions of the maximum erosion depth at full scale.

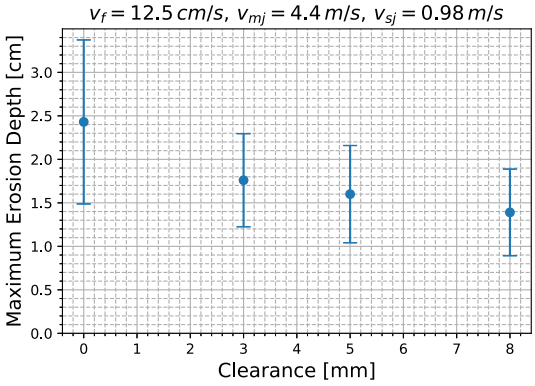

Fig. 13. Effect of bottom clearance on the erosion depth.

The maximum erosion depth e_m can be converted to an erosion rate v_e using the following relationship:

$$v_e = \frac{e_m}{t}, \tag{6}$$

where t is the time over which the bed is exposed to the flow, which can be estimated using the following relationship:

$$t = \frac{d}{v_f}, \tag{7}$$

in which $d = 150$ mm represents the bed distance instantly exposed to the flow, which was measured from photos obtained by a high-speed camera.

Employing Froude scaling, one can estimate the full-scale maximum erosion depth as follows (the subscript s indicates small scale, while the subscript f indicates full scale):

$$e_{m,f} = v_{e,f} \cdot t_f = 4 \cdot v_{e,s} \cdot t_s = 4 \cdot t_s \cdot e_{m,s} \tag{8}$$

Here, we provide an example of the erosion depth that can be predicted for reasonable operational conditions using our experimental results and Equation (8). Based on Test 4, for a full-scale scenario with a forward velocity of 25 cm/s, a clearance of 12 mm, and main and secondary jet velocities of 8.8 m/s and 2.0 m/s, respectively, the maximum erosion depth is determined to be 70 mm. Notably, this value falls within the anticipated range, as reported by Boschen-Rose et al. [7].

6. Turbidity currents generated by spilling water

The phenomenon of spilling water behind the collector generates a turbidity current that moves in the opposite direction of the collector. Videos are recorded for each experimental run to visually assess the characteristics of this current. Additionally, an Ultrasonic Velocity Profiler (UVP) equipped with one transducer operating at 4 MHz is employed to measure vertical velocity profiles at a specific position (3500 mm a way from the rear of the clay tray). The transducer is held in position by a custom-built holding house with a 30° angle relative to the normal of the flume bottom as presented in Fig. 14, which also displays the turbidity current of Test 4.

To facilitate comparison between experiments, velocity profiles of turbidity current bodies were analyzed at the moment when the front of the current was 4000 mm away from the rear of the clay tray. Fig. 15 shows time-averaged vertical velocity profiles obtained from the UVP data for two experimental runs. Using such a velocity profile, it is possible to determine associated characterizing parameters. Among these parameters, the characterizing height h [m] represents the thickness of the turbidity current, while the layer-averaged velocity U [m/s] reflects the average velocity of the current across its depth. These parameters can be determined using the following relations [13]:

$$U h = \int_0^{z_\infty} u \, dz, \tag{9}$$

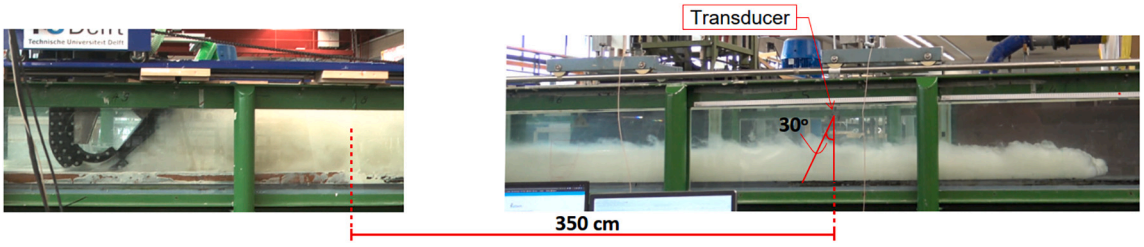

Fig. 14. Photos showing turbidity currents generated by the spilling water behind the collector head and the position of the UVP transducer measuring the flow velocity of the body of the turbidity current.

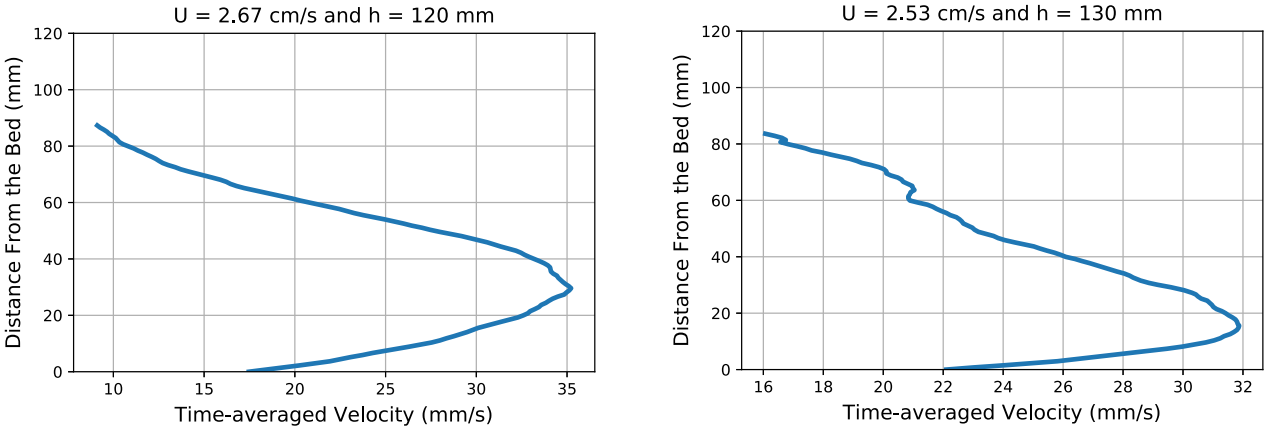

Fig. 15. Time-averaged velocity profiles of Experiment 4 (left) and Experiment 7 (right) when the front of the current was 4000 mm away from the rear of the clay tray. The profiles are a result of averaging 3 successive instantaneous profiles (sampling frequency = 8.4 Hz).

Table 3
Characterizing height h (m) and layer-averaged velocity U (m/s) determined using the velocity profiles obtained by the UVP.

Test #	Qc [L/s]	Front velocity [cm/s]	U [cm/s]	h [mm]	U·h [cm^2/s]
4	10.5	1.77	2.7	120	32.0
5	10.5	1.78	2.8	136	37.9
6	10.5	1.67	2.8	129	35.5
7	10.5	1.86	2.5	130	32.9
8	4.4	1.63	2.7	93	25.1
9	7.4	2.45	4.3	193	82.8
10	9.1	1.91	2.9	148	42.5

$$U^2 h = \int_0^{z_\infty} u^2 \, \mathrm{d}z, \tag{10}$$

where u [m/s] is locally averaged streamwise flow velocity, z [m] is upward-normal coordinate and z_∞ is the height at which the local velocity u is zero. The quantities h and U are obtained by solving the system of Equations (9)-(10).

Additionally, the front velocity of the turbidity currents was determined for each experiment from the video recordings. The analysis of front velocities and layer-averaged velocities of the body of turbidity currents reveals their clear correlation with Q_c (see Table 3); an increased Q_c results in decreased turbidity current velocities (Tests 4, 9, and 10). This indicates that a larger Q_c results in less water spillage behind the collector head and thus smaller flow velocities, which is in line with the observation of Alhaddad and Helmons [2]. It is also clear that U is almost the same in Tests 4, 5, 6 and 7, because Q_c is the same.

6.1. Discussion

The analysis of our experimental results demonstrates that the thickness of the cohesive sediment layer eroded by a Coandă-effect-based collector is logarithmically proportional to the flow impinging force. This indicates that the force exerted by the flow on the sediment bed is the crucial parameter to optimize for minimizing sediment pick-up. Once minimized, the amount of sediment discarded behind the collector through the collection duct will be minimized, consequently alleviating the associated environmental impact.

The sediment-water mixture is recirculated over the secondary-jet duct in the actual complete collector. With regard to sediment erosion, based on the findings of our study, it is recommended to keep the secondary-duct jet with a minimised flow velocity to minimise erosion depth. It should be noted that the optimal operational conditions of the collector should eventually be determined based on minimal environmental impact, together with satisfactory pick-up efficiency.

A clear distinction between our experiments and real-life conditions lies in our use of a sediment bed devoid of nodules, unlike the actual environment. The impact of the presence of nodules remains unexplored. Nevertheless, our hypothesis suggests that the presence of nodules would likely decrease sediment erosion depth. The collector initially gathers existing nodules, and subsequently, the sediment faces the flow, resulting in a reduced exposure time compared to a scenario with a bare sediment bed. This reduced exposure time is expected to lead to shallower erosion depths, as previously detailed in this article.

With regard to turbidity currents, our study shows that an increased flow rate in the collection duct, Q_c, results in a slower turbidity current generated behind the collector head. In this respect, it should be noted that increasing Q_c may result in a more energetic turbidity current resulting from discarding the sediment-water mixture at the rear of the collector through a discharge duct. Given that these two turbidity currents will eventually interact behind the collector, it is recommended to investigate which turbidity current should be more dampened from an environmental standpoint.

7. Conclusion

In order to facilitate the development of a Coandă-effect-based hydraulic collector with minimal environmental stresses, we conducted a series of small-scale experiments investigating the erosion and suspension of cohesive sediment caused by such a collector. These experiments involved testing various operational conditions, demonstrating the impact of each operational parameter on clay erosion, which is in agreement with former experiments on sand erosion. Our experimental results demonstrate an inverse relationship between the collector's forward velocity and the erosion depth. Furthermore, an increase in the main/secondary jet velocity contributes to a larger erosion depth. Besides, when the collector's underside is closer to the sediment bed, a larger portion of the sediment layer is exposed to the water flow, resulting in a greater erosion depth. A thorough analysis of the experimental outcomes confirmed a logarithmic relationship between erosion depth and the flow impinging force applied on the clayey bed. This suggests that minimizing this force is necessary to minimize erosion depth. Our analysis also shows that an increased flow rate in the collection duct results in a slower turbidity current generated behind the collector head. Another key finding of this study is that the presence of a secondary-jet duct itself leads to a decreased erosion depth, underscoring the importance of minimizing the flow velocity through it.

CRediT authorship contribution statement

Said Alhaddad: Writing – review & editing, Writing – original draft, Visualization, Supervision, Project administration, Methodology, Investigation, Formal analysis, Conceptualization, Data curation. **Mohammed Suleman:** Writing – original draft, Visualization, Methodology, Investigation, Formal analysis, Data curation, Conceptualization. **Alex Kirichek:** Writing – review & editing, Supervision, Resources, Project administration, Conceptualization, Methodology. **Claire Chassagne:** Writing – review & editing, Supervision, Project administration.

Declaration of competing interest

The authors declare that they have no known competing financial interests or personal relationships that could have appeared to influence the work reported in this paper.

Data availability

Data will be made available on request.

Acknowledgement

The authors would like to thank the Hydraulic Engineering Laboratory of Delft University of Technology for providing the necessary laboratory facilities to conduct our experiments.

Appendix A. Cross-sectional profiles of all experiments

Figs. 16–29 depict the cross-sectional profiles corresponding to all experiments listed in Table 1.

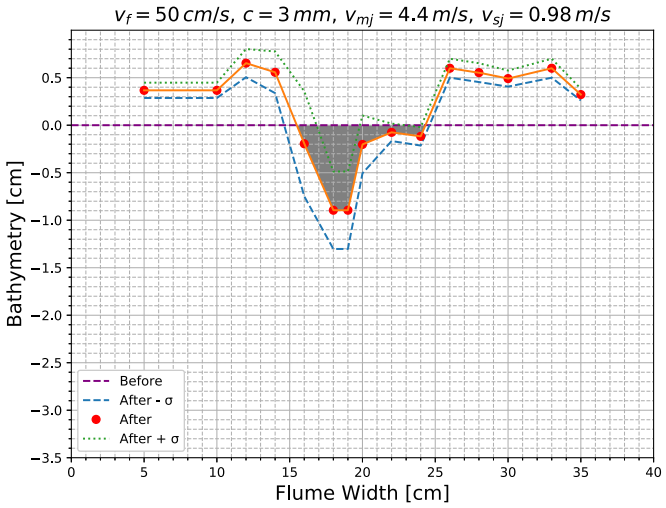

Fig. 16. Cross-sectional profile of Experiment 1.

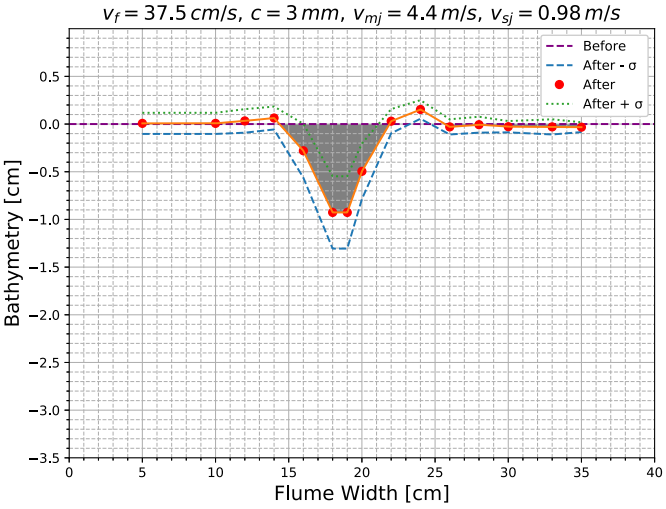

Fig. 17. Cross-sectional profile of Experiment 2.

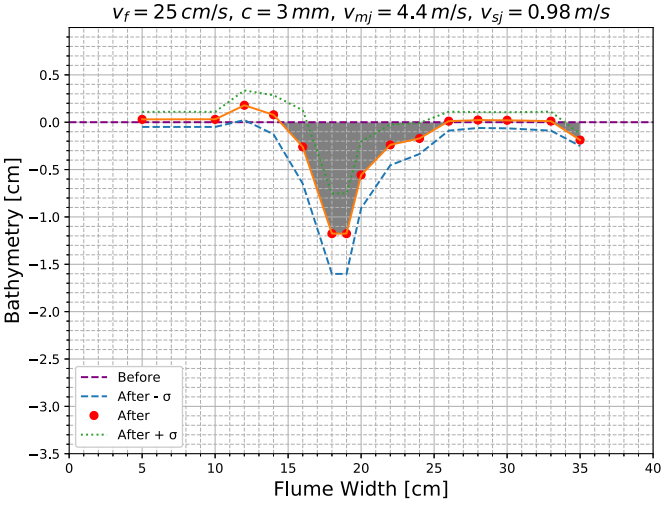

Fig. 18. Cross-sectional profile of Experiment 3.

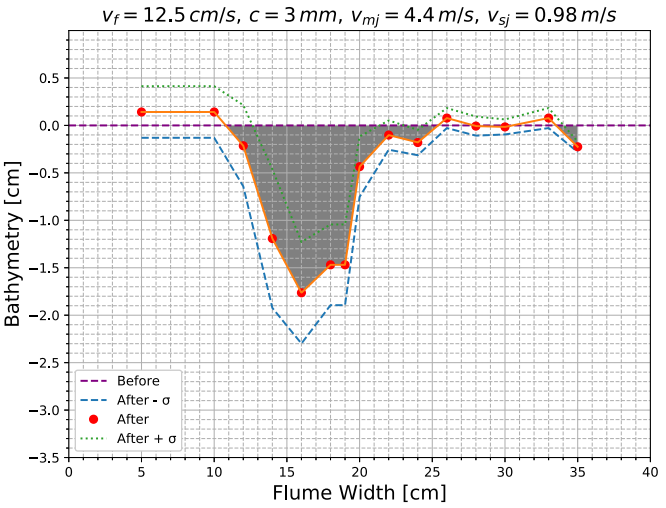

Fig. 19. Cross-sectional profile of Experiment 4.

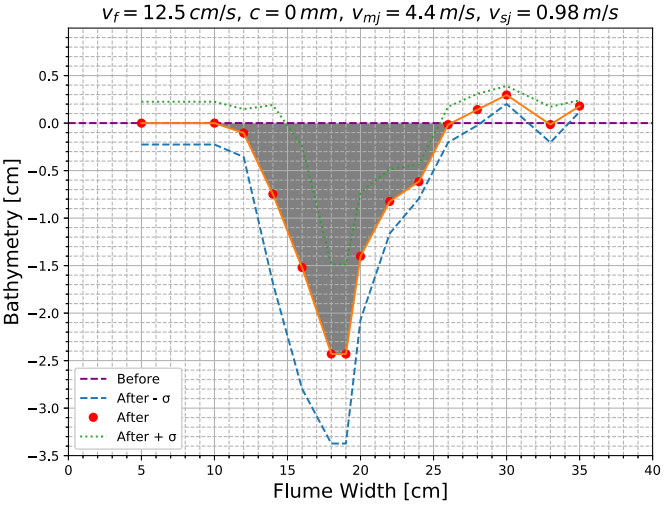

Fig. 20. Cross-sectional profile of Experiment 5.

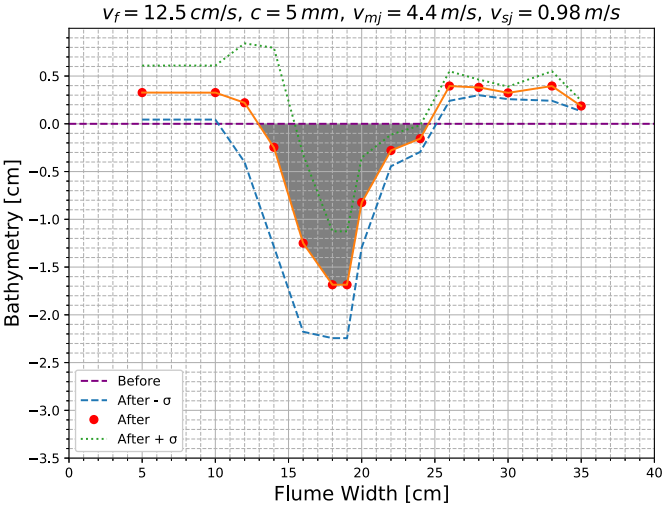

Fig. 21. Cross-sectional profile of Experiment 6.

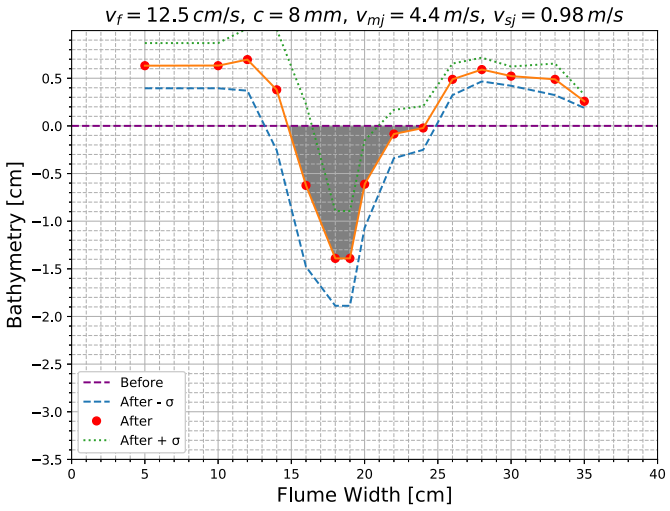

Fig. 22. Cross-sectional profile of Experiment 7.

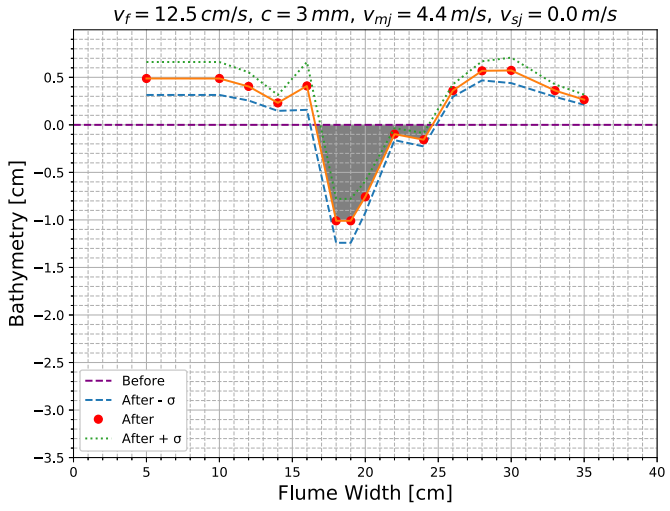

Fig. 23. Cross-sectional profile of Experiment 8.

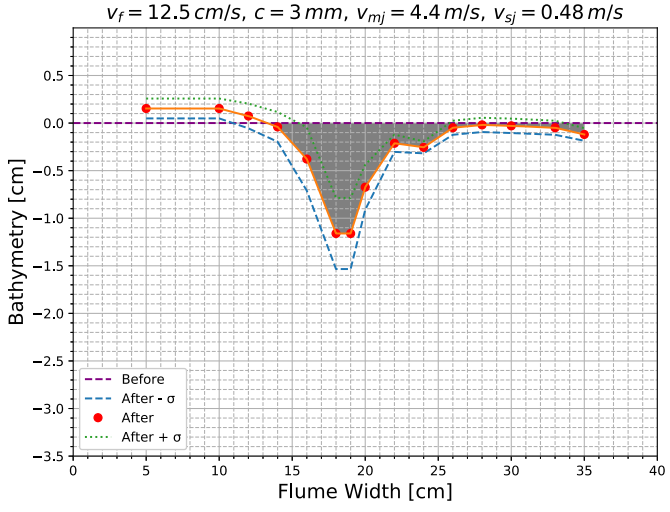

Fig. 24. Cross-sectional profile of Experiment 9.

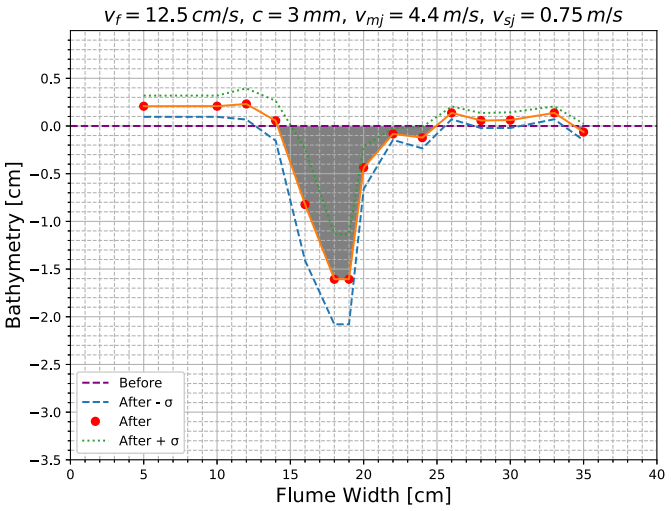

Fig. 25. Cross-sectional profile of Experiment 10.

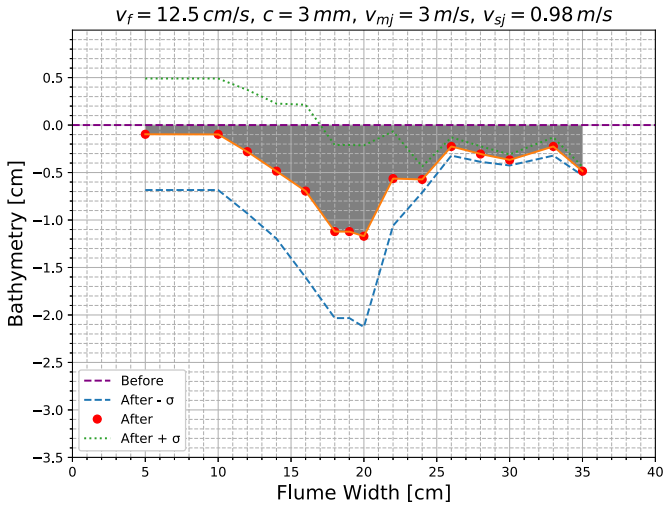

Fig. 26. Cross-sectional profile of Experiment 11.

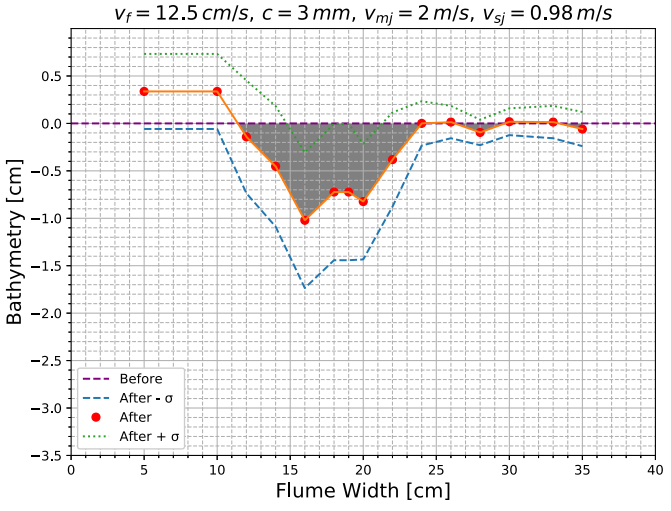

Fig. 27. Cross-sectional profile of Experiment 12.

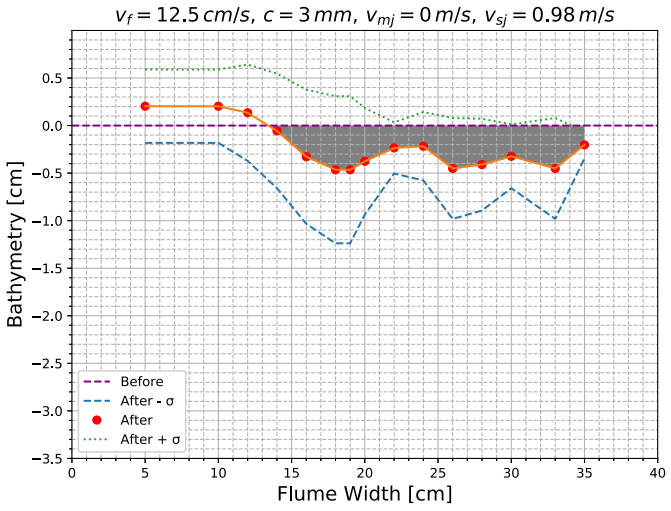

Fig. 28. Cross-sectional profile of Experiment 13.

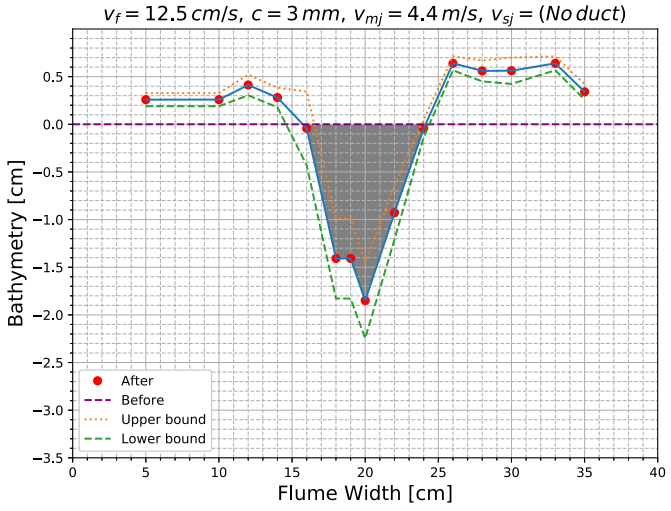

Fig. 29. Cross-sectional profile of Experiment 14.

References

[1] S. Alhaddad, M. Elerian, Mitigating suspended-sediment environmental pressure in subsea engineering through colliding turbidity currents, Results Eng. 21 (2024) 101916.
[2] S. Alhaddad, R. Helmons, Experimental investigation of sediment erosion generated by coandă-effect-based polymetallic-nodule collectors, in: Proceedings of the World Dredging Congress WODCON XXIII, Copenhagen, Denmark, May 2021, pp. 16–20.
[3] S. Alhaddad, R. Helmons, Sediment erosion generated by a coandă-effect-based polymetallic-nodule collector, J. Mar. Sci. Eng. 11 (2023) 349.
[4] S. Alhaddad, G. Keetels, D. Mastbergen, C. van Rhee, C.H. Lee, E.P. Montellà, J. Chauchat, Subaqueous dilative slope failure (breaching): current understanding and future prospects, Adv. Water Resour. 104708 (2024).
[5] S. Alhaddad, D. Mehta, R. Helmons, Mining of deep-seabed nodules using a coandă-effect-based collector, Results Eng. 17 (2023) 100852.
[6] S. Alhaddad, D. Weij, C. van Rhee, G. Keetels, Stabilizing and destabilizing breaching flow slides, J. Mar. Sci. Eng. 11 (2023) 560.
[7] R. Boschen-Rose, H. Stigter, C. Taymans, Z. Mravak, Environmental impact assessment (eia) components for test mining up to prototype level (trl 6), in: Blue Nodules Deliverable Report D1.7, 2020.
[8] M. Elerian, S. Alhaddad, R. Helmons, C. van Rhee, Near-field analysis of turbidity flows generated by polymetallic nodule mining tools, Mining 1 (2021) 251–278.
[9] GSR, Environmental Impact Statement: Small-scale testing of nodule collector components on the seafloor of the Clarion-Clipperton Fracture Zone and its environmental impact, Technical Report, 2018.
[10] J.R. Hein, A. Koschinsky, T. Kuhn, Deep-ocean polymetallic nodules as a resource for critical materials, Nat. Rev. Earth Environ. 1 (2020) 158–169.
[11] M. Iatrou, G. Ferentinos, G. Papatheodorou, D.J. Piper, E. Tripsanas, Anthropogenic turbidity current deposits in a seismically active graben, the Gulf of Corinth, Greece: a useful tool for studying turbidity current transport processes, in: Submarine Mass Movements and Their Consequences: 3 International Symposium, Springer, 2007, pp. 149–157.
[12] H.U. Oebius, H.J. Becker, S. Rolinski, J.A. Jankowski, Parametrization and evaluation of marine environmental impacts produced by deep-sea manganese nodule mining, Deep-Sea Res., Part 2, Top. Stud. Oceanogr. 48 (2001) 3453–3467.
[13] G. Parker, Y. Fukushima, H.M. Pantin, Self-accelerating turbidity currents, J. Fluid Mech. 171 (1986) 145–181.
[14] T. Peacock, R. Ouillon, The fluid mechanics of deep-sea mining, Annu. Rev. Fluid Mech. 55 (2022).
[15] I. Reba, Applications of the coanda effect, Sci. Am. 214 (1966) 84–93.
[16] K.J. Schulz, J.H. DeYoung, R.R. Seal, D.C. Bradley, Critical mineral resources of the United States: economic and environmental geology and prospects for future supply, Geol. Surv. (2018).
[17] A. Shakeel, A. Kirichek, C. Chassagne, Rheology and yielding transitions in mixed kaolinite/bentonite suspensions, Appl. Clay Sci. 211 (2021).
[18] R. Sharma, Deep-Sea Mining: Resource Potential, Technical and Environmental Considerations, Springer, 2017.
[19] Z. Yue, G. Zhao, L. Xiao, M. Liu, Comparative study on collection performance of three nodule collection methods in seawater and sediment-seawater mixture, Appl. Ocean Res. 110 (2021).
[20] G. Zhao, L. Xiao, Z. Yue, M. Liu, T. Peng, W. Zhao, Performance characteristics of nodule pick-up device based on spiral flow principle for deep-sea hydraulic collection, Ocean Eng. 226 (2021) 108818.